Pivotal Contribute of EPR-Characterized Persistent Free Radicals in the Methylene Blue Removal by a Bamboo-Based Biochar-Packed Column Flow System

Filippo Zanardi,[a] Federica Romei,[a] Mario Nogueira Barbosa Junior,[b] Sidnei Paciornik,[b] Paola Franchi,[c] Marco Lucarini,[c] Anna Turchetti,[c] Lorenzo Poletti,[d] Silvana Alfei,*[e] and Omar Ginoble Pandoli*[e, f]

Water remediation with biomass derivatives has attracted attention for its sustainable impact on the earth. Chemical procedures for new adsorbent and active biomaterials must be implemented to remove organic pollutants more efficiently. Herein, we obtained a sustainable, environmentally, and low-cost biochar from bamboo *Dendrocalamus giganteus* (BBC, B400) by thermal treatment at 400 °C without physical and chemical pre- and post-treatments. By electron paramagnetic resonance (EPR), we determined the quantification and ageing of persistent free radicals (PFRs, 10^{16}–10^{19} spins/g) present in BBC over time. We demonstrated the removal efficiency (R%) of B400 against methylene blue (MB) aqueous solutions without and with different concentrations of H_2O_2 using a novel B400-packed column-flow system. Results demonstrated that the MB removal efficiency via physical adsorption and chemical degradation strongly depended on the concentration of carbon-centred PFRs and their stability over time. Collectively, a reduced concentration of PFRs and their full passivation by proper treatments led to a remarkable loss of MB removal

efficiency, thus evidencing that a PFR-mediated radical degradation mechanism was predominant in the MB removal process. Experiments with t-butanol alcohol (TBA) on aged B400 as a radical scavenger of the hydroxyl radical ($^\bullet$OH) have evidenced the critical role of PFRs in generating reactive oxygens species (ROSs) in solution, which catalysed the oxidative degradation of MB. Kinetics studies carried out on removal efficiency data vs time by all experiments established that the MB removal profiles of fresh B400 were best described by a pseudo-second order (PSO) kinetic model, thus suggesting that chemical mechanisms such as electron transfer reactions and PFRs-mediated degradation were the main contributors to MB removal. On the contrary, MB removal profiles of aged B400 with reduced or insignificant content of PFRs best fitted kinetic models, which describe physical absorption and diffusional nor radical processes, which led to a lower removal efficiency. These findings will be helpful for potential pilot and large-scale experiments to remove a wide range of contaminants in water.

1. Introduction

Developing sustainable carbon materials from the pyrolysis of lignocellulosic biomass has attracted significant attention in the last 15 years, with different applications such as biochar (BC)-based functional materials.[1,2] Depending on the physical parameters, elemental composition, and chemical structures, the applications of BC platforms can be tuned for environ-

mental remediation,[3,4] industrial wastewater treatment,[5] soil amendment,[6] removal of heavy metals,[7] water purification[8] and catalysis.[9,10] The carbonaceous material obtained by pyrolysis at 200–1000 °C is mainly gained from different vegetal, wood and animal biomass feedstocks.[11] More recently, bamboo-based biochar (BBC) and activated bamboo biochar (ABBC) have increasingly attracted the interest of researchers due to the nonpareil physicochemical characteristics of bamboo plants,

[a] F. Zanardi, F. Romei
Department of Chemistry and Industrial Chemistry, University of Genoa, Via Dodecaneso, 31, 16146 Genoa, Italy

[b] M. N. B. Junior, S. Paciornik
Departamento de Engenharia Química e de Materiais, Pontifícia Universidade Católica do Rio de Janeiro (PUC-Rio), Rua Marquês de São Vincente, 225, 22451-900 Rio de Janeiro, Brazil

[c] P. Franchi, M. Lucarini, A. Turchetti
Department of Chemistry "Giacomo Ciamician", University of Bologna, Via P. Gobetti 85, 40129 Bologna, Italy

[d] L. Poletti
Department of Chemical, Pharmaceutical and Agricultural Sciences, University of Ferrara, Via L. Borsari, 46, 44121 Ferrara, Italy

[e] S. Alfei, O. G. Pandoli
Department of Pharmacy, University of Genoa, Viale Cembrano, 4, 16148 Genoa, Italy
E-mail: alfei@difar.unige.it

[f] O. G. Pandoli
Departamento de Química, Pontifícia Universidade Católica do Rio de Janeiro (PUC-Rio), Rua Marquês de São Vincente, 225, 22451–900 Rio de Janeiro, Brazil
E-mail: omar.ginoblepandoli@unige.it
omarpandoli@puc-rio.br

ChemCatChem
Research Article
doi.org/10.1002/cctc.202401042

Chemistry
Europe
European Chemical
Societies Publishing

their abundance, and their very fast growth.[12] BC's chemical and physical activation, providing activated biochar (ABC), helps to increase its specific surface absorption area and porosity. Upon activation, additional functional groups or heteroatoms can be introduced on BC to improve the chemical interaction with metals and organic molecules, thus allowing their removal from wastewater and/or soil. These secondary chemical procedures necessarily increase the cost of BC production and the residual chemical waste. Thus, the most environmentally friendly and low-cost BC is preferred for minor foot-printing in scaling up carbonaceous material industrial production.

In recent years, it has been demonstrated the presence of persistent free radicals (PFRs) in BC particles and their crucial role in catalysing the degradation of aromatics[13–15], pharmaceutical pollutants[16,17] and organic dyes.[18,19] Specifically, BC, in addition to removing different xenobiotics by adsorption phenomena into its microporous structure, would degrade them via PFRs-dependent oxidative reactions. Redox properties of plant biomass-derived BC,[20–22] and their mechanisms in the advanced oxidation process (AOP) have been reported.[23–25] Recently, the formation and evolution mechanism of PFRs in BC from biomass feedstocks pyrolysis[26,27] and lignocellulose-derivates[28] has been disclosed. Anyway, while BC-associated PFRs and their participation in BC-catalysed removal of contaminants have been studied from the year 2014, only four recent works have been reported on the presence of PFRs and their use for pollutant remediation in bamboo-based BC (BBC).[11,29–32] If the benefits and the environmental applications of the PFRs have been demonstrated, the environmental fate, risk, and impact of the PFRs are less documented as potential new classes of pollutants.[33–35] Identifying PFRs with carbon or oxygens-centred radicals and their quantification in solid BC is possible by electron paramagnetic resonance (EPR).[34] Still, a more straightforward colourimetric assay for rapidly quantifying PFR in BC is also possible using tetramethyl benzidine (TMB) as an organic dye mediator.[36]

It should be noted that, although there is a lot of work on the BC capability to remove organic and inorganic contaminants from water or soil, all the abovementioned papers have used batch tests to demonstrate it. Only one work has proven the reduction of 4-nitrophenol using carbonised wood impregnated with bimetallic nanoparticles as a monolithic continuous-flow microreactor.[37] Furthermore, as recently reviewed about bamboo as a bio-absorbent,[38] the contribution of adsorption phenomena has been shown with homogenous and tedious discontinuous methods. Only microwave-modified bamboo charcoal (BC-MW) has been used as a biosorbent in batch (1 mg$_{dye}$/50 mg$_{BC}$) and fixed-bed column with BC and BC-MW. In this case, hydrophobic, π–π and electrostatic interactions were mainly responsible for the adsorption of organic dyes.[39]

Herein, we present a pyrolysis procedure for a PFR-rich bamboo-derived biochar (BBC) without any chemical or physical treatment. For the first time, we have demonstrated the pivotal contribution of PFRs in BBC for methylene blue (MB) efficient removal through a continuous column-packed flow system. Long-term degradation stability was determined for 3 BBC-packed columns, using MB aqueous solutions (2.5×10^{-5} M) with different amounts of H$_2$O$_2$. EPR-assisted monitoring of an 18-month-aged BC was performed to follow the decreasing concentration of PRFs over time due to atmospheric oxygen exposure (or quenching over time) and the influence of this event on the MB degradation efficiency by BC. Finally, we have demonstrated the chemical degradation of MB by the hydroxyl radicals ($^{\bullet}$OH) generated by BC's PFR using t-butyl alcohol (TBA) as a scavenger of the ROS. Kinetics studies were carried out on MB removal profiles obtained by different experiments by fitting the experimental data of removal efficiency (%) vs time with six mathematical kinetic models to investigate and assess the main mechanisms that governed the MB removal processes by B400. Results from this study unequivocally demonstrated that in the performed experiments, PFRs were the main contributors to the MB removal via a PFRs-mediated oxidative degradation by ROS, and that their reduction or absence led to a dramatic decrease in the MB removal efficiency by B400.

Materials and Methods

Materials and Sample Preparation

Bamboo-derived biochar (BBC) was produced from 4-year-old giant bamboo (*Dendrocalamus giganteus*) cut 2 m away from the root, at the PUC-Rio campus. Bamboo culms were cut and cleaned with hot water, dried for 24 hours in the oven at 60 °C, cut into 6 mm diameter and 20 cm length sticks, and stored under vacuum until use.[40] Before the pyrolysis, the sticks were cut into cubes in the middle of the bamboo wall with dimensions ca. 1 cm^3 and dried until a stable weight was reached. The carbonisation and/or graphitisation (pyrolysis) was performed in an OTF 1200X series tube furnace (MTI) in a temperature range between 200 °C and 1000 °C under N$_2$ atmosphere. For more details, the same procedure was used in our previous work.[41] The resulting bamboo-based monolithic carbons were used without chemical pre- and post-treatment. The pulverised materials were obtained with a Retsch MM 400 ball mill with a total collision time of 30 min and a frequency of 15/s. The powdered materials were used for Raman spectroscopy (RS), elemental composition analysis (EA), and electron paramagnetic resonance *(EPR). The complete analysis by inductively coupled plasma-optical emission spectrometry (ICP-OES), thermal gravimetric analysis (TGA), X-ray powder diffraction (XRPD), transmission electron microscopy (TEM), X-ray microtomography (μCT), and X-ray photoemission spectroscopy (XPS) analysis was disclosed in our previous work.[41]

Biomass Chemical Characterisation

Electron Paramagnetic Resonance (EPR)

Electron paramagnetic resonance (EPR) spectra were recorded by Bruker ELEXSYS E500 spectrometer equipped with an NMR Gaussmeter for the calibration of the magnetic field and a frequency counter for the determination of g-factors. The EPR analysis of bamboo-based biochar (BBC) was conducted 16 months after its generation, sealed, and stored at room temperature. Four months later, after exposure to atmospheric oxygen during experimental procedures, the EPR analysis was repeated to determine the decrease in the spin concentration of BBC. The analysis was conducted on natural bamboo (BNAT) and samples treated at different pyrolysis temperatures (B200-B1000). Bamboo

ChemCatChem

Research Article
doi.org/10.1002/cctc.202401042

Chemistry Europe
European Chemical
Societies Publishing

powders stored for 16 months not exposed and after exposition (4 months) to the atmospheric oxygen were weighed directly (c.a. 5–10 mg) into sealed glass capillaries inside EPR tubes, accurately positioned inside the cavity, and the analyses of the solids were carried out at room temperature. Measurement conditions: modulation amplitude = 1.0 G; conversion time = 81.92 ms; time constant = 81.92 ms; modulation frequency = 100 kHz; field width = 100 G, microwave power = 0.80 mW; and microwave frequency = 9.30 GHz.

Measured g-factors were corrected with respect to that of a standard sample of a perylene radical in concentrated H_2SO_4 (g = 2.00258) and checked against the measured value for 2,2-diphenyl-1-picrylhydrazyl radical (DPPH) at the solid state (g = 2.0036).[42]

The concentration of radicals present in the powders, depending on the pyrolysis temperature, was determined by comparing the double integral of the EPR signal with that of a reference solution of tetramethyl pyperidin-N-oxyl radical (TEMPO, Sigma-Aldrich) in an inert solvent such as hexane, using the signal from a piece of synthetic ruby fixed to the inside wall of the microwave cavity as a sensitive reference.[43]

EPR analyses in solution were recorded in the presence of 5,5-dimethyl-1-pyrroline-N-oxide (DMPO). According to the reactions shown in Scheme 1, the DMPO was used as the ideal spin-trapping reagent to identify ROS ($O_2^{\bullet-}$, $HOO^\bullet$, $ROO^\bullet$ and $^\bullet OH$) generation.
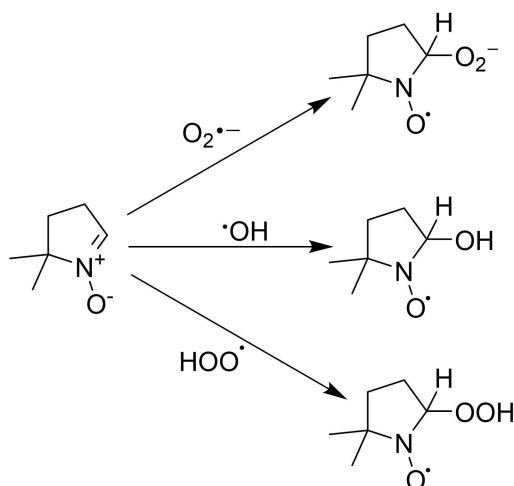
Scheme 1. Scheme of DMPO-adducts generating by the reaction of transient radicals with DMPO.

The different obtained persistent nitroxides give rise to specific EPR signals that allow them to be differentiated. For the EPR experiment with DMPO, 2 mg of any sample was weighed in an Eppendorf, and 200 μL of 0.2 M DMPO in 0.02 M PBS buffer was added. The samples were sonicated for 5 minutes, and then, after the solid had settled for 20 minutes, the analysis was carried out.

For the EPR experiment with DMPO and hydrogen peroxide, 1 μL of H_2O_2 2.94 M was added to the prepared sample, obtaining a final H_2O_2 concentration of 15 mM. The samples were sonicated for 5 minutes, and then, after the solid had settled, the analysis was carried out.

Measurement conditions: modulation amplitude = 1.0 G; conversion time = 81.92 ms; time constant = 81.92 ms; field width = 80 G, modulation frequency = 100 kHz; microwave power = 6.35 mW; and microwave frequency = 9.30 GHz.

Elemental Composition Analysis (EA) and Raman spectroscopy

An elemental analyser (Flash 2000) was employed to determine the elemental composition of C, H and N for the natural and pyrolyzed bamboo samples. Confocal Raman Renishaw with a laser excitation of 488 nm was employed to determine the modification of the lignocellulosic polymer during the graphitisation process.

Column-Packed Flow System First Set-Up

Figure 1 shows a schematic experimental setup and an image of the laboratory system.

For the column-packed flow experiments, Omnifit™ EZ chromatography columns (Sigma Aldrich, Milan, Italy) were used, with one fixed and one adjustable endpiece (Ø = 8.8 mm, 150 mm length). Glass beads (150–200 μm) were obtained from Merck (Milan, Italy), while methylene blue (MB, CAS 61-73-4) was from ISOFAR (Rio de Janeiro, Brazil). Each column was filled with 5 g of glass beads and 10 mg of B400. The solid mixture for 3 columns was obtained initially by weighing 15 g of glass beads and 30 mg of B400. Due to losses in the transfer procedure, 20% more than the theoretical loading was weighed.

Three MB solutions (2.5×10^{-5} mol/L) with different amounts of H_2O_2 were injected into the 3 columns containing the same quantity of B400 with a volume/weight ratio of 1 mL $_{solution}$/1 mg $_{B400}$. From a reservoir, 10.1 mL of MB solution was pumped with a peristaltic pump into the columns (1–3) at a 0.5 mL/min flow rate. Table 1 collects the detailed experimental data.
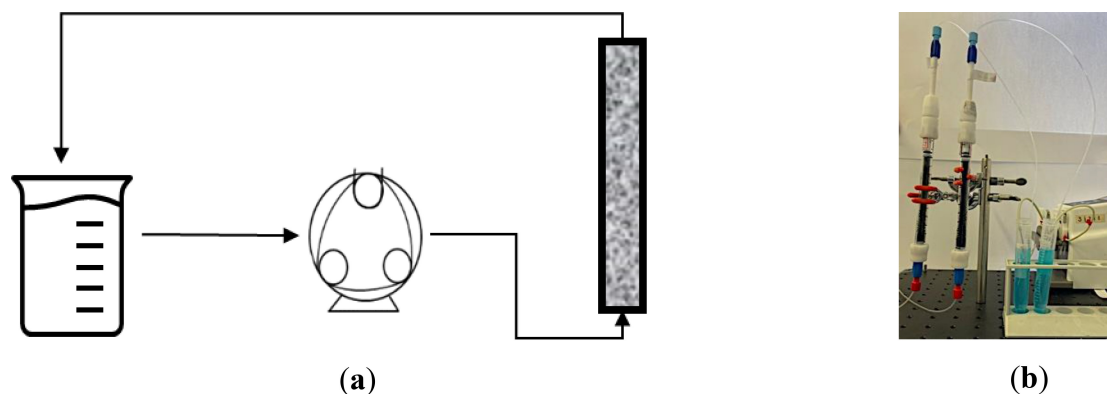

Figure 1. Scheme of the B400-packed column system with a reservoir of MB solution, a peristaltic pump and Omnifit™ EZ biochar-packed column (a); image of the laboratory experimental set-up with three B400-packed columns containing 10 mg B400 and 5 g of glass beads (b).

ChemCatChem

Research Article
doi.org/10.1002/cctc.202401042

Chemistry
Europe
European Chemical
Societies Publishing

Table 1. Experimental data and solution compositions in the MB removal experiments.

Column	MB solution [a] (mL)	Water (μL)	H₂O₂ 0.025 M (μL)	H₂O₂ 0.125 M (μL)	MB/ H₂O₂ (ratio)	B400/H₂O₂ (mg/mmol)
1	10	100	N.R.	N.R.	N.R.	N.R.
2	10	N.R.	100	N.R.	1:10	400:1
3	10	N.R.	N.R.	100	1:50	80:1

[a] 2.5×10^{-5} mol/L; N.R. = not reported.

MB degradation was monitored by a Fiber Optic UV-Vis Spectrometer System Ocean Optics USB 2000 (Ocean Optics, Inc., Dunedin, FL, USA) in 3 mL quartz cuvettes for 2 hours. At 30-, 60- and 120-minute intervals, an aliquot of about 1.5 mL was withdrawn from the reservoir, and its absorbance (Abs) was measured at 663 nm. The Abs values were used to calculate the cumulative MB removal percentage (R%) at the fixed time points by a proper equation reported in Section 3. R% values were plotted vs. time to obtain the MB cumulative removal efficiency (%) graph over time. This experiment represented one cycle of ten carried out to assess the long-term efficiency of the three columns. After every cycle, the columns were reused in the subsequent experiment with fresh solutions up to 3 experiments (3 cycles) per day. Experiments were performed in triplicate, and the results were expressed as mean± standard deviation (SD).

The same experiments were later re-performed using the aged B400 exposed to air for four months during the previous ones, detecting a significant reduction in the removal efficiency by aged B400 due to a significant reduction in the PFRs concentration (spin/g) as confirmed by a repeated PFR analysis. While the PFRs' lifetime under vacuum appears infinite, they can react with atmospheric molecular oxygen when exposed to air, resulting in decay with time.[44,45] In this case, cycles did not go over 5 since degradation was minimal already at cycle 5. In addition to oxygen, the persistence and stability of PFRs are synergistically influenced by other individual environmental factors such as humidity, occasional organic pollutants, and pH variations.[46] Humidity plays a crucial role in both the formation and stability of PFRs.[47] In environments with relative humidity of approximately 33%, H₂O can quench PFRs and reduce their half-life by 3.5 times.[48] PFRs exhibit higher stability and persistence in a hypoxic environment, and an oxygen content of about 6% can reduce the intensity of PFRs signal close to zero.[46] Although the direct relationship between pH and free radical stability isn't explicitly stated, the principles of electron donation, delocalization, and steric effects, which are known to

affect PFRs stability, can be modulated by pH changes. This suggests that pH can impact the stability of PFRs.[49,50] Anyway, because of the potential industrial applications of BBC, the control of the atmosphere parameters should not be a factor to be considered to keep the costs of large-scale production low.

Finally, an experiment with a solvent scavenger (tert-butanol alcohol, TBA) was implemented to observe the quenching effect on ROS generated in solution, thus leaving only the adsorption phenomena as a possible reason for MB removal efficiency by B400. The alcoholic solution used in the scavenger experiments was prepared from a stock solution of MB in water (5×10^{-4} mol/L) and diluted with TBA to achieve the final solution used in the experiment (2.5×10^{-5} mol/L).

Column-Packed Flow System Second Set-Up using Passivated B400

To determine the adsorption contribution of the bio-adsorbent B400, we set up the new flow experiment configuration shown in Figure 2.

Before the MB removal experiments, already aged B400, which demonstrated a significantly reduced concentration of PFRs in the second EPR analyses, was packed into columns 1–3, and its passivation was performed by recirculating 200 mL of H₂O₂ 0.025 M at a flow rate of 0.5 mL/min. The columns were also irradiated with UV light during the treatment with H₂O₂ for approximately 4 hours. Through this process, we attempted to accelerate the inactivation of the radicals still present in B400 to determine its absorption contribution.[51,52] In the subsequent experiments of MB removal by the passivated aged B400, 100 mL of MB solutions (2.5×10^{-5} mol/L), not containing (column 1) or added with H₂O₂ (columns 2 and 3) as in the previous experiments, was pumped at 0.5 mL/min flow rate and recollected continuously into 10 test tubes every 20 minutes. The increasing MB concentration in the 10 fractions of approx-
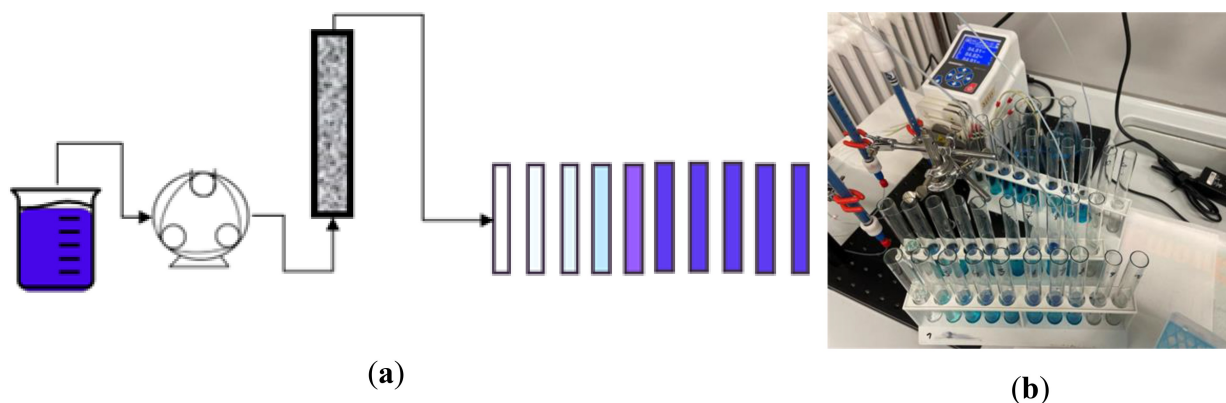

(a)　　　　　　　　　**(b)**

Figure 2. Schematic representation of a reservoir of MB solution, peristaltic pump, Omnifit™ EZ column with fix-bed BC and recollected fractions (a); image of the same laboratory set-up (b).
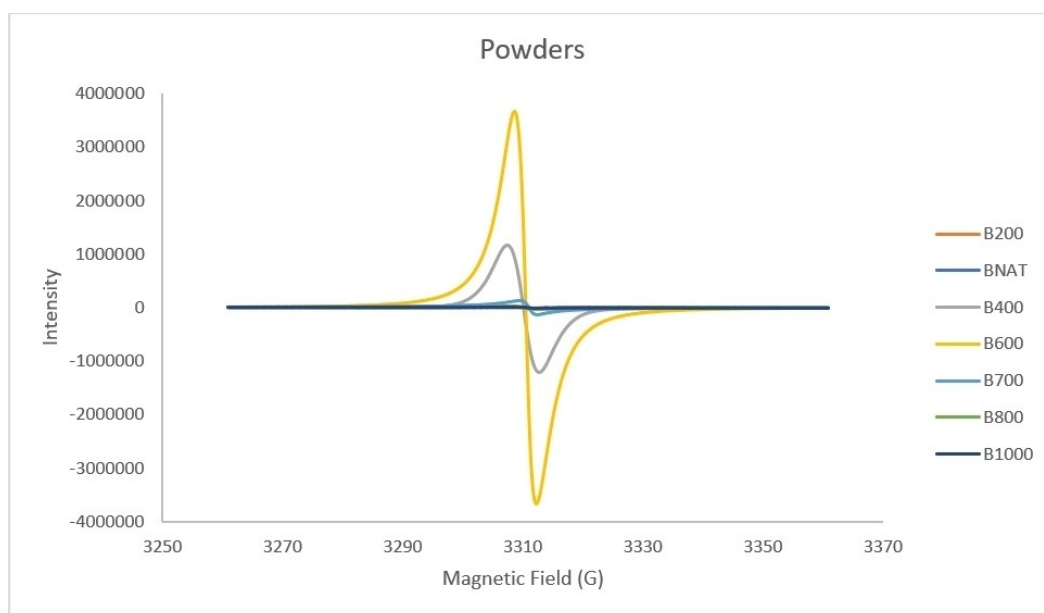
ChemCatChem

Research Article
doi.org/10.1002/cctc.202401042

Chemistry
Europe
European Chemical
Societies Publishing

Figure 3. EPR signals were detected in the examined bamboo pyrolyzed powders not exposed to oxygen for 16 months.

imately 10 mL was monitored by UV-vis analysis, and the decreasing MB removal efficiency percentage was determined.

2. Results and Discussion

2.1. EPR Analyses

EPR analyses revealed that the number of radicals in the powders could depend on the pyrolysis temperature. In particular, the presence of radicals was irrelevant in BNAT and B200. At the same time, it became remarkably significant in B400 (1.93×10^{19} spins/g), reached its maximum in B600 (7.74×10^{19} spins/g) and decreased in B700 and B800 until it became negligible again in B1000. The spin concentration is in accordance with the findings with other woody lignocellulosic biomass under different pyrolysis biomass.[53] The observed results are summarised in Figure 3 and Table 2. The g-factor values ranged from 2.0028 to 2.0032. So, the type of persistent free radicals (PFRs) in the examined powders was mainly consistent with sp^2 carbon-centred radicals, which, according to the literature, have a g-factor value of around 2.0030.[42]

The preliminary results of MB removal with B600 were the worst compared to B400. Thus, we started characterising the removal efficiency of B400, considering the importance of reducing the energy and time costs consumed by the BC-producing process. It is worth noticing that B400 was submitted to a thermal treatment where cellulose and hemicellulose were degraded but remained stable in the lignin polymers. At 600 °C, all the lignocellulose polymers were degraded with a total biomass carbonisation. These phase transformations were evident in TGA, XPS, FT-IR and Raman, as discussed elsewhere.[54] In Figure S1a and b in Supplementary Materials, we have reported the Raman spectra and elemental composi-

Table 2. Concentrations, g-factor and line width of persistent free radicals (PFRs) in BCs obtained at different pyrolysis temperatures.

Entry	Code	Line Width (Gauss)	PFRs concentration (Spins/g)	g factor[a]
1	BNAT	6.85 ± 0.1	6.55×10^{15}	2.0029 ± 0.0001
2	B200	6.25 0.1	1.47×10^{17}	2.0032 ± 0.0001
3	B400	5.29 ± 0.1	1.93×10^{19}	2.0030 ± 0.0001
4	B600	3.92 ± 0.1	7.74×10^{19}	2.0030 ± 0.0001
5	B700	2.90 ± 0.1	8.80×10^{18}	2.0028 ± 0.0001
6	B800	4.37 ± 0.1	1.85×10^{18}	2.0029 ± 0.0001
7	B1000	3.10 ± 0.1	3.40×10^{15}	2.0028 ± 0.0001

[a] g-factor values were corrected against the perylene radical cation in concentrated sulphuric acid (g = 2.00258). TEMPO (3 mM) in cyclohexane (g-factor = 2.00617) was used as an external standard. 15 µL were taken to have approximately the same volume of tube occupied by the powders.

tion. Raman analyses from 800 to 2000 cm^{-1} confirmed the formation of the D and G band, at 1355 and 1602 cm^{-1}, respectively, characteristics of the graphitisation process of the lignocellulosic polymers in the bamboo biomass. The intensity ratio of these two bands is related to the disorder of the carbon material. The higher I_D/I_G ratio of 0.62 of B600, compared to the $I_D/I_G = 0.49$ of B400, indicates an increased graphitisation and lower disorder of the graphene layers.[54] Indeed, during the formation of B600, all the lignocellulose polymers were carbonised with a better order of graphenic and turbostratic carbons. This evidence was corroborated by XPS and FT-IR results.[54] In the elementary analysis, the increase of about 1.5 times in the C/H ratio in B600 compared to B400 was due to the incremental thermal treatment. These observations about the chemical composition and graphitisation degree of B400 and

ChemCatChem

Research Article
doi.org/10.1002/cctc.202401042

Chemistry Europe
European Chemical
Societies Publishing

B600 could be one of the reasons for their different efficiency in MB removal.

2.1.1. EPR Analysis in the Presence of DMPO

The generation of ROS in the presence of BNAT and B400 powders in water suspension was investigated using DMPO as a spin trap. The coupling constants of the unpaired electron with the paramagnetic nuclei of nitrogen (a_N) and hydrogen in beta position (a_H) in the DMPO-adducts are characteristics of the captured radicals. Only hydroxyl radicals ($^{\bullet}OH$) were detected through a specific four-line EPR signal corresponding to DMPO-OH ($a_{N=}a_{H=}14.84$ G), formed by the reaction of $^{\bullet}OH$ with DMPO (Scheme 1). In the absence of H_2O_2 the amount of $^{\bullet}OH$ radical

trapped by DMPO, DMPO-OH ($a_N=a_H=14.84$ G), was relatively limited in BNAT powder. It was almost double in the presence of B400 powder as can be evidenced by comparing the intensity of the signals related to DMPO-OH produced in both cases (Figure 4a and b). The relative intensity of the second line of the DMPO-OH spectrum in the BNAT had a value of 2.7×10^4, while that in the B400 spectrum had a value of 4.8×10^4. In both cases, we can also observe the presence of an alkyl adduct in DMPO, generically referred to as DMPO–R ($a_N=15.39$ G, $a_H=22.83$ G). However, these weak signals disappeared when hydrogen peroxide was added (Figure 4c and d). As shown in Scheme 2, the biochar acts as an "electron shuttle" to transfer electrons to oxygen, forming superoxide anion ($-O_2$), which dismutates to H_2O_2. The PFR catalyses the formation of $^{\bullet}OH$.
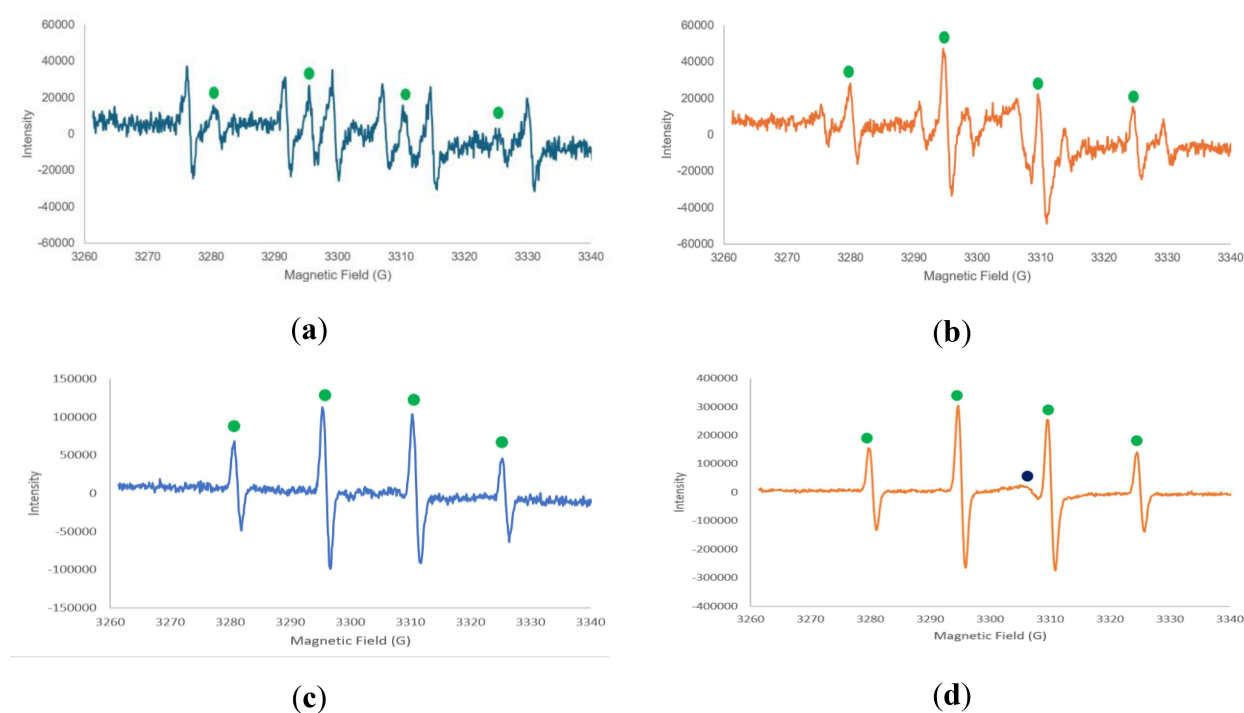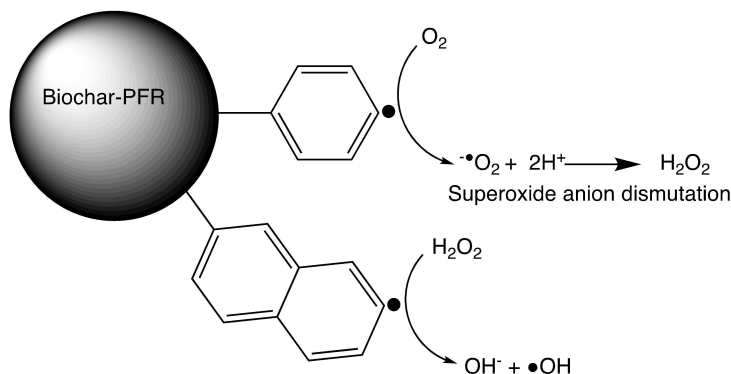

Figure 4. EPR spectra of DMPO (0.2 M in 0.02 M PBS) without H_2O_2, in the presence of (a) BNAT and (b) B400 powders. EPR spectra of DMPO (0.2 M in 0.02 M PBS) with 15 mM of H_2O_2, in the presence of (c) BNAT and (d) B400 powders. Green ●: DMPO–OH adduct. Blue ●: PFRs.

Scheme 2. The hypothesis of ROS generation in water induced by biochar-PFR. The PFR "electron-shuttle" catalyses the formation of superoxide anion, hydrogen peroxide and hydroxyl radical.

2.1.2. EPR Analysis in the Presence of DMPO and Hydrogen Peroxide

The EPR spectra recorded adding H_2O_2 to the systems under investigation (Figure 4c and d), showed only the four-line signal ($a_{N} = a_{H} = 14.84$ G), due to the coupling of the unpaired electron with paramagnetic nuclei of nitrogen and hydrogen in beta position in the DMPO-OH radical adduct. Different nitroxide radical adducts formed by the reaction of other ROS with DMPO (specific multiple line signal with $a_{N} \neq a_{H}$) were not observed. In the spectrum recorded in the presence of B400 (Figure 4d), we noted also a minimal trace of persistent carbon-centred free radicals (PFRs) (g factor $= 2.0030$), probably due to a minimum amount of powder remaining in suspension and not ultimately settled. The $^{\bullet}OH$ radical entrapped by DMPO increased by 4 times in the spectrum obtained in the presence of BNAT and by 7 times in the spectrum obtained in the presence of B400, respectively, as demonstrated by the intensity of the signals attributed to the DMPO-OH adduct. Comparing in Figure 4a–c and 4b–d, the intensity of the second line of the DMPO-OH increased from $2.7{\times}10^4$ to $1.13{\times}10^5$ in the spectrum obtained for the sample containing BNAT and from $4.7{\times}10^4$ to $3.4{\times}10^5$ in the spectrum of the sample containing B400. Comparing the second peaks in the BNAT and B400 spectra, an increase in intensity from $1.13{\times}10^5$ to $3.40{\times}10^5$ was observed. These findings indicate that H_2O_2 can be produced and decomposed to $^{\bullet}OH$ and support the selection of B400 for MB removal in a fixed-bed column system.[55]

2.2. Flow Experiments Results

2.2.1. Long Term Removal Efficiency of Columns Packed with Fresh B400

The MB removal from MB solutions flowed through the packed columns were followed spectroscopically.[56,57] Since early ex-periments had evidenced that the maximum removal was reached already after 120 minutes flowing, we measured the absorption of the organic dye solution for 2 hours after 30, 60 and 120 minutes for cycle, for a total of 10 cycles. The MB removal given by adsorption into the adsorber and/or chemical degradation due to PFR was monitored by measuring the absorbance change at 663 nm in the MB solution under treatment, and the removal percentage (R%) was determined through the following Equation (1).

$$\%R = \frac{[A_o - A_t]}{A_o} \times 100 \qquad (1)$$

In (1), A_0 is the absorbance of the mother solution, and A_t is its absorbance after a time t flowing through the packed column.[56] The R% profiles of the three columns during 10 cycles showed in Figure 5, evidenced that the MB was removed to a higher extent in presence of H_2O_2 (columns 2 and 3). For all the experiments with and without H_2O_2, the R% was maintained above 90% for the first 4 cycles. As the number of cycles progressed, the increase in H_2O_2 concentration led to the maintenance of higher R% for a higher number of cycles (column 3). Anyway, the R% remained around 50% even at the tenth cycle (20 hours).

2.2.1.1. Kinetics Study

As recently reported for tetracycline (TC) removal by PFRs-containing BCs, degradation and adsorption mechanisms could coexist in the pollutants removal processes by BC and BC/H_2O_2 systems.[29] So, the experimental data shown in Figure 5 were further studied by fitting them with the most common mathematical kinetic models, to investigate the main kinetics and physicochemical reactions (physical absorption or chemical degradation by PFRs action) governing the MB removal over-time during the ten cycles. To this end, the ten cycles were
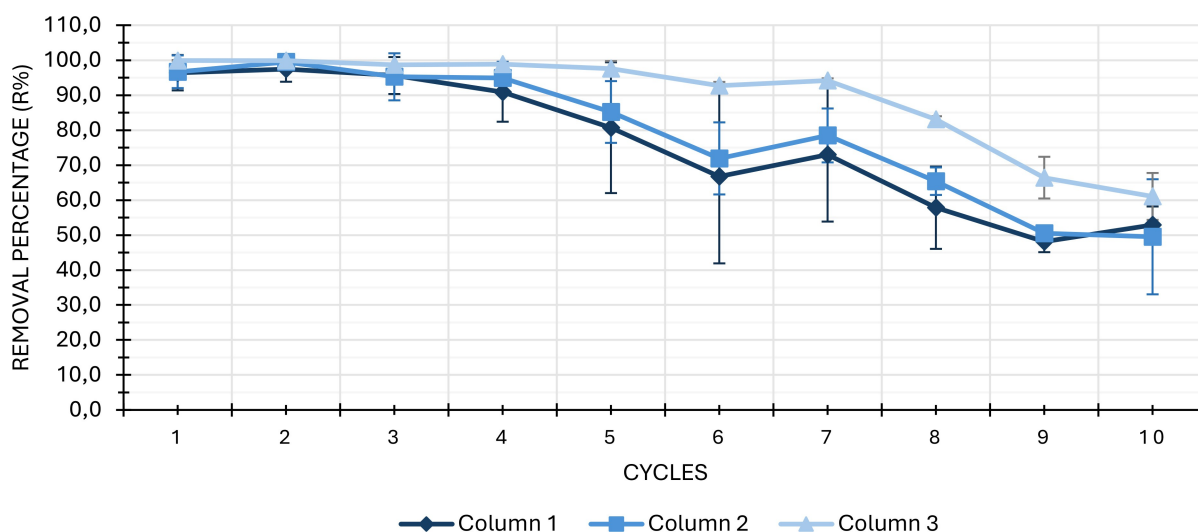

Figure 5. Long-term removal stability expressed as removal percentage for the 3 packed columns without and with different amounts of H_2O_2 into MB solutions: (Column 1) MB solution, (Column 2) solution of MB/$H_2O_2 = 1:10$, and (Column 3) solution MB/$H_2O_2 = 1:50$.

ChemCatChem

Research Article
doi.org/10.1002/cctc.202401042

Chemistry
Europe
European Chemical
Societies Publishing

Table 3. Variables are to be reported on the x and y axes to obtain the dispersion graphs of mathematical models considered in this study and the equations expressing them.

Model	X Axis	Y Axis	Equation
Zero-order	Times	R%	$R\%(t) = K_0 \times t + RE\%(t_0)$
First-order	Times	Ln (residual %)	$Ln[R\%(t)] = [R\%(t0)] + \frac{K1}{2.303} \times t$
PSO	Times	t/R% (t)	$t/R\%(t) = (1/R\%_{eq}) \times t + 1/[K_{PSO} + (R\%_{eq})^2$
Higuchi	SRT [a]	R%	$R\%(t) = K_H \times t^{1/2}$
Korsmeyer-Peppas	Ln (times)	Ln (R%)	$Ln[R\%(t)] = n_{KP} \times Ln(t) + Ln(K_{KP})$
Hixson-Crowell	Times	Cubic root (residual %)	$\sqrt[3]{1 - F\%(t)} = 1 - KHC \times t$

PSO=Pseudo second order; [a] square root of times; R% (t) is the removal percentage on time t; R% (t$_0$) is the removal percentage at the beginning (t = t$_0$); K$_0$ is the zero-order constant; R%$_{eq}$ is the removal percentage at equilibrium; K1 is the first order constant; K$_{PSO}$ is the equilibrium constant velocity of the PSO kinetic model; K$_{KP}$ is the transport constant of the Korsmeyer-Peppas model; n$_{KP}$ (also called diffusional or transport exponent) provides information on the possible mechanism(s) governing the process under study; F% (t) is the cumulative fraction percentage of removal on time t; K$_{HC}$ is the Hixson-Crowell constant; K$_H$ is the Higuchi kinetic constant.

converted in times (120 min per cycle for a total of 20 hours). The adopted kinetic models included zero order, first order, pseudo-second order (PSO), Higuchi, Korsmeyer–Peppas and the Hixson–Crowell mathematical models.[58,59] Such models have been explained in detail in Section S1 of Supplementary Materials. Table 3 shows how the dispersion graphs associated with the models were graphically obtained and their equations.

The linear regressions and their equations were provided by Microsoft Excel software 365 using the ordinary least square (OLS) method. The dispersion graphs, the associated linear regression lines and related equations have been shown in Figure S2–S7 (Supplementary Materials). The coefficients of determination (R^2) associated with all the equations have been reported in Table S1 and were considered as the parameters to determine which model best fits the R% data according to the literature.[58] R^2 values evidenced that the PSO model well fit the removal efficiency data (R^2 0.9475, 0.9269 and 0.9288) of all columns (Figure S4), even if the Hixson Crowell model (Figure S7) was the model that best described the removal process by columns 3 (R^2 0.9495). According to Table 3, for columns 1 and 2, whose MB removal profiles best fit the PSO kinetic model, the PSO constant (K$_{PSO}$) was determined by the intercept of the blue and light blue equations in Figure S3, while the equilibrium R% (R%$_{eq}$), in this case the minimum R% achieved after 20 hours of work (R%$_{20\ PSO}$) was predicted by their slope. Otherwise, for column 3, whose removal process was better described by the Hixson Crowell model, the Hixson Crowell constant (K$_{HC}$) was the slope of the very light blue equation in Figure S7. Since the PSO model sufficiently well fit the removal data of all columns, K$_{PSO}$ and R%$_{20\ PSO}$ were also calculated for column 3 using the very light blue equation in Figure S4. Similarly, since the Hixson Crowell model sufficiently well described the MB removal by columns 1 and 2, K$_{HC}$ was determined by the blue and light blue equations in Figure S7 for comparison purposes. All the determined kinetic parameters have been inserted in Table 4. A higher value of K within a model corresponded to a lower rate of removal efficiency loss. The experimental values of removal efficiency (R%) at the maximum working time of 20 hours (R%$_{20\ EXP}$), corresponding to the minimum R% for all columns observed in the performed

Table 4. Kinetic parameters for PSO and Hixson Crowell models that best fit the experimental data describing the loss of removals efficiency (%) over 20 hours of work for the three columns reported in Figure 5.
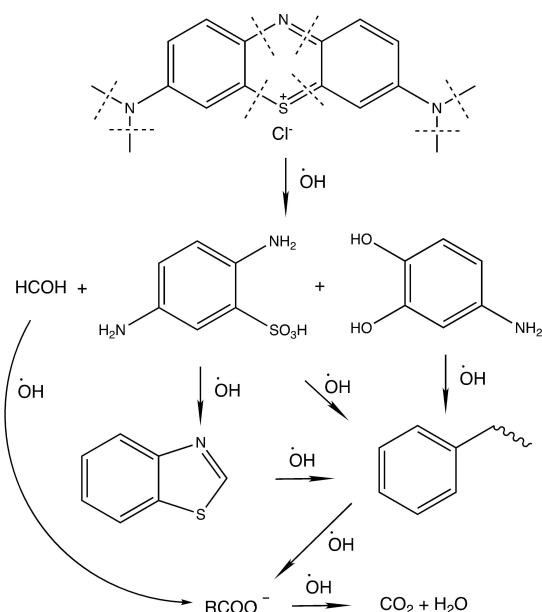
Column	R%$_{20\ EXP}$	R%$_{20\ PSO}$	K$_{HC}$ [a]	K$_{PSO}$ [b]
1	52.9	47.2	0.1447	2212
2	49.5	47.8	0.1563	2269
3	61.0	62.5	0.1678	3881

EXP = Experimental after 20 h 10 cycles; PSO = pseudo-second order; HC = Hixson Crowell; [a] Hixon Crowell kinetic constants expressing the rate of the removal efficiency loss of the three columns; [b] pseudo-second order kinetic constants expressing the rate of the removal efficiency loss of the three columns A higher value of K within a model corresponded to a lower rate of removal efficiency loss.

experiment, were also included in Table 4 and compared with those predicted by the PSO (R%$_{20\ PSO}$) kinetic model.

In the removal processes governed by the PSO kinetics, the velocity limiting step is considered chemical adsorption, including adsorption through the sharing or exchange of electrons between the adsorbent and the adsorbed, as in radical degradations, or electrostatic interactions.[60,61] In this regard, since the removal efficiency experimental data of columns 1, 2 and 3 well fit the PSO kinetic model, it can be assumed that the overall MB removal by B400 occurred mainly via the degradative oxidation action of ROS, formed by PFRs-mediated electron transfer reactions to O$_2$ (column 1) or to O$_2$ and H$_2$O$_2$ (column 2 and 3) as reported.[62,63] Scheme 3 represents the oxidative pathway degradation of MB operated by the generated ROS species •OH.[63]

Manly, upon the necessary physical absorption of MB onto B400, PFRs were the main contributors to its removal over time due to oxidative degradation, acting as donors, acceptors, and/or shuttles of electrons.[64] The good agreement of R% values after 20 hours of treatment predicted by the model and the experimental ones, especially for column 3, used to treat MB solutions with high H$_2$O$_2$ concentration as ROS source, further confirmed this assumption. Moreover, although a loss in the removal efficiency over time, due to B400 saturation and radicals' decay, was observed for all columns, it was more

ChemCatChem

Research Article
doi.org/10.1002/cctc.202401042

Chemistry Europe
European Chemical
Societies Publishing

Scheme 3. MB oxidative cascade mediated by the ROS species •OH. Adapted from[63]

evident for columns 1 and 2, especially over 480 minutes of treatments. This is because they were used to treat MB solutions without H_2O_2 or with a lower concentration of H_2O_2, thus being minor in the possibility of ROS production by PFRs action. Specifically, in these columns, physical absorption, affected by rapid saturation, was less supported by ROS action in the MB removal than in column 3, thus determining a higher reduction in the removal efficiency after the same time.

This observation further confirmed that the long-term removal efficiency of B400 was based more on radical degradation than physical absorption. According to K values by both models, the MB removal efficiency loss over time was more rapid for column 1, followed by column 2 and then column 3, which lost efficiency significantly slower than the other columns, as also observable in Figure 6. As for the Hixson Crowell model, which also well fits the MB removal profiles over time of all columns and was even superior to the PSO model for column 3, it describes a system where the cube root of removal efficiency on time t is linearly related to that time. Processes well described by Hixson Crowell kinetics are typically characterised by systems whose surface alters over time.[65] The fact that the MB removal by B400 in column 3, which was used to filter the MB solution with a high concentration of H_2O_2, best fits this model could make us think of a significant surface alteration of BBC over time by its oxidative action.

To best investigate the possible mechanisms of MB removal by B400, a similar kinetic study was applied to the data of graphs obtained by plotting R% determined at 30, 60 and 120 minutes within a single cycle vs time for cycles 5 and 6 (second week of experiments) (Figure S8, in Supplementary Material). We selected cycles 5 and 6 because they represent a critical phase of the overall experiment, where a significant inflexion in MB removal efficiency occurred, especially for columns 1 and 2 (Figure 6). We assumed that, in these cycles, the coexistence of both mechanisms (radical degradation and physical absorption) should have been more obvious. The values obtained for R^2 have been included in Table S2, which evidenced that the MB removal profiles over time well fit both PSO, and Korsmeyer-Peppas kinetics. A minor fitting, especially for columns 2 and 3, was evidenced for the Higuchi model. The regression graphs, the linear regressions and the related equations of these models have been shown in Figure S9–S11 in Supplementary Materials. As reported above, in removal processes that fit PSO kinetics, electron transfer reactions, electrostatic interactions, and hydrogen bond formation are the main mechanisms governing the process. Differently, in those fitting the Higuchi model, they are physical diffusional mechanisms. Concerning those fitting the Korsmeyer Peppas model,
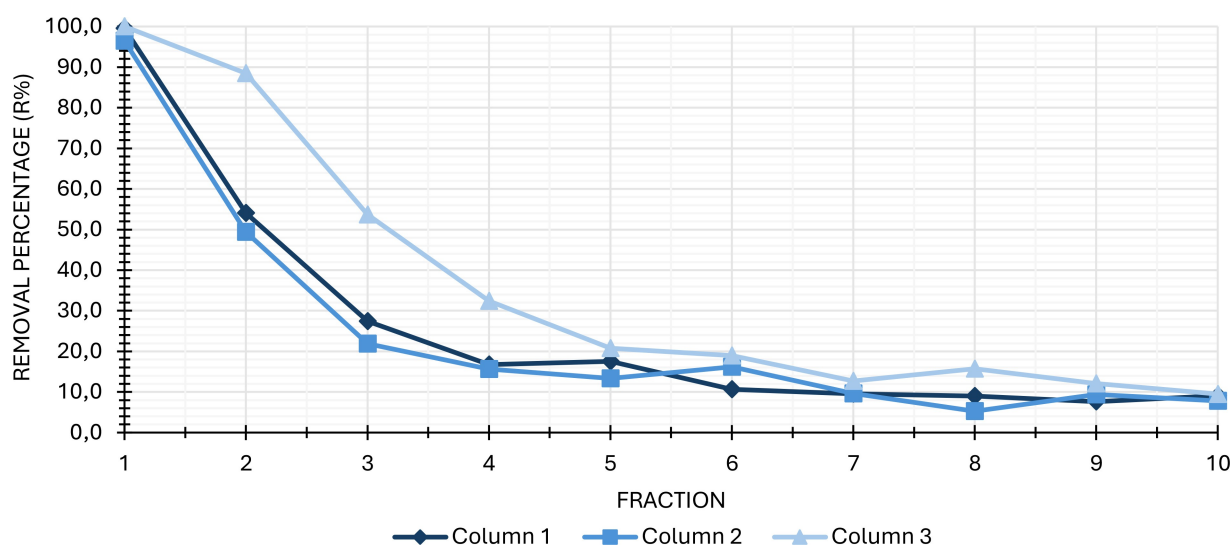

Figure 6. MB removal efficiency in fractions subsequently collected for the 3 packed columns without and with different amounts of H_2O_2 into MB solutions: (Column 1) MB solution, (Column 2) solution of MB/$H_2O_2 = 1:10$, and (Column 3) solution MB/$H_2O_2 = 1:50$.

ChemCatChem

Research Article
doi.org/10.1002/cctc.202401042

**Chemistry
Europe**
European Chemical
Societies Publishing

the main mechanisms could be diffusional or more complex not chemical processes (Case II or Super Case II transport) depending on the value of the diffusional or transport exponent n_{KP}.[66] The fact that our experimental data fit well both PSO and Korsmeyer Peppas models establishes that the MB removal by B400 was governed by both radical and physical absorption/ diffusional mechanisms. Based on R^2 values, the MB removal by all columns in cycle 5 and column 3 in both cycles best fit the PSO model. Differently, the MB removal by columns 1 and 2 in cycle 6 best fitted the Korsmeyer-Peppas model. These findings confirmed a predominance of degradative oxidation by PFRs-mediated increasing of ROS in cycle 5 for all columns. In cycle 6, only the MB removal profile by column 3 best fits the PSO model, thus indicating an MB removal via radical mechanisms. This could be due to the high content of H_2O_2 in MB solutions, which allowed a sufficient ROS concentration despite a reduced radical decaying concentration over time. On the contrary, the MB removal by columns 1 and 2, in the absence or presence of a lower concentration of H_2O_2 as a source of ROS, best fit the Korsmeyer-Peppas model, thus demonstrating a predominance of diffusional or more complex physical mechanisms. In this case, the reduced concentration of radicals, due either to their decay over time and/or to a shortage of ROS sources, led to a significant reduction in the MB removal efficiency concerning column 3 (66.8% column 1 and 71.9% column 2 vs. 92.7% column 3). In this regard, the Higuchi model, which describes absorption processes based on physical diffusional mechanisms, fits quite well only the MB removal by column 1, where the absence of H_2O_2 in MB solutions strongly reduced the possibility of ROS formation in the presence of PFRs, which decays over time. In this case, ROS formation could occur only by PFRs-mediated electron transfer to airy oxygen, thus reducing the ROS contribution in the MB removal by oxidative degradation. According to the equations in Table 3, the kinetic parameters of all models were determined and inserted in Table 5. PSO kinetic parameters were determined as previously described, n_{KP} and K_H were provided by the slope of equations in Figure S10 and S11, respectively, while K_{KP} values were computed by the intercept of equations in Figure S10. The experimental maximum R% values measured at time 120 min (R%$_{120\,EXP}$) were also included in Table 5 and compared with those obtained by PSO model (R%$_{120\,PSO}$).

All R% values determined at 120 minutes provided by the PSO model were in perfect agreement with experimental ones with an R^2 value of 0.9905 (Figure S12), thus confirming the suitability of PSO equation to model the MB removal data. As expected, kinetic constants by all models, expressing the removal efficiency rate of the three columns within two consecutive cycles of 120 minutes, established that all columns were more rapid in MB removal in cycle 5 than in cycle 6, thus confirming a progressive decay of PFRs and their essential role in the MB degradation process. Additionally, columns 3 in both cycles demonstrated the highest removal rate, rationally due to the highest concentration of H_2O_2, which helped an improved PFRs-mediated production of ROS, which in turn supported the MB removal by oxidative degradation. Finally, the transport coefficient n_{KP} values provided by Korsmeyer-Peppas gave additional information on the possible intimate mechanisms governing the MB removal by physical absorption in cycle 6 (columns 1 and 2). Since was $n_{KP} < 0.45$ (absolute value), it can be assumed that, when physical absorption occurred, the MB removal followed a Fickian diffusional mechanism.

2.2.2. Biomass Removal Efficiency over Time by Passivated Column by H_2O_2 and UV Treatment

Figure 6 shows the decreasing MB removal efficiency of columns 1–3 filled with aged and passivated B400 over time. MB solutions flowed through columns 1–3 and had the same composition as those used in the previous experiments. In this experiment, in which B400 wholly deprived of PFRs and ROS was used, we attempted to extrapolate the B400 not radical absorption contribution in the MB removal process.

The maximum absorbance capacity after 50 mL was calculated by determining the mg of MB in 50 mL and subtracting it from the residual amount of MB obtained from the absorbance measurements of the fractions. The residual mass of MB was calculated for each fraction, and then these residual masses were added up to fraction 5. The difference between the residue and the theoretical mg of MB in 50 mL measured the MB absorbed. This data was divided by the amount of biomass in each column in grams to obtain the maximum adsorption capacity of 25.71 mg$_{dye}$/g$_{BC}$ for column 3, in the presence of H_2O_2 (Table 6). The comparison of several activated bamboo-based biochar used for MB removal ranged a maximum absorption capacity from 50 to 700 mg$_{dye}$/g$_{BC}$. All the BCs were activated with different chemical agents (NaOH, KOH, NaClO, KHCO$_3$, KMnO$_4$) and modified with acrylic acid, cross-linking, and nitrogen doping by urea.[38]

As evident in Figure 6, the biomass for all the columns (1–3) had a high absorption of MB in the first fractions collected every 10 mL. After 50 mL (fraction 5), the exiting solutions

Table 5. Kinetic parameters for PSO, Higuchi and Korsmeyer-Peppas models, which best fit the experimental data of removal efficiency (%) over time (120 minutes) of the three columns, reported in Figure S8, in Supplementary Materials.

Column	R%$_{120\,EXP}$	R%$_{120\,PSO}$	K_{PSO}[a]	K_H[b]	K_{KP}[c]	n_{KP}
1 V	93.9	96.2	9238	8.8708	32.2	0.2275
1 VI	84.3	87.0	7558	7.9044	22.9	0.2747
2 V	91.4	92.6	8546	8.6466	48.9	0.1331
2 VI	79.2	80.6	6483	7.3658	29.7	0.2039
3 V	96.0	97.1	9400	9.0998	48.8	0.1443
3 VI	93.5	95.2	9040	8.8214	43.1	0.1639

EXP=Experimental; PSO = pseudo-second order; H=Higuchi; KP=Korsmeyer Peppas; [a] pseudo-second order kinetic constants expressing the rate of the removal efficiency of the three columns over time for cycles V (120 minutes) and VI (120 minutes) within a total of ten cycles; [b] Higuchi kinetic constants expressing the rate of the removal efficiency of the three columns over time for cycles V (120 minutes) and VI (120 minutes) within a total of ten cycles; [c] Korsmeyer-Peppas kinetic constants expressing the rate of the removal efficiency of the three columns over time for cycles V (120 minutes) and VI (120 minutes) within a total of ten cycles.

Table 6. Maximum absorbance capacity after 50 ml for columns 1,2 and 3.	
Column	Maximum absorbance capacity after 50 mL (mg_{dye}/g_{BC})
1	19.00
2	17.45
3	25.71

demonstrated almost the same concentration as entering the columns. Column 3, which contained a higher concentration of H_2O_2, maintained a significantly higher degradation efficiency than columns 1 and 2 for a longer time and up to fraction 4, after which its efficiency dramatically decreased at columns 1 and 2 levels, as reported in Table 7. However, columns 1 and 2, already from the third fraction, showed a remarkably lower degradation percentage ($< 30\%$).

2.2.2.1. Kinetic Study

Also, in this case, the possible mechanisms governing the MB removal and the loss of removal efficiency of B400 over time were investigated by carrying out a kinetic study on data reported in Figure 6, like those previously described. To this end, the fractions were converted into times, being each fraction 20 minutes (Figure S13). Table S3 collects the R^2 values determined for all kinetic models applied. R^2 values evidenced that the Korsmeyer-Peppas model best fit all columns' removal efficiency data (R2 0.9712, 0.9251 and 0.9396) (Figure S14). This finding established that in this experiment, the decreasing MB removal in the fractions subsequently collected was governed mainly by physical absorption/desorption mechanisms, with a minimal contribution of PFRs, probably due to a reduced number of radical active sites in consequence of B400 treatment with H_2O_2. According to Table 3, n_{KP} and K_{KP} values were determined by the slope and intercept of the equations in Figure S14 for all columns. The determined kinetic parameters have been inserted in Table 7, together with the experimental R% values determined at the maximum time (200 minutes) considered (R%$_{200\,EXP}$). A higher value of K corresponded to a lower rate of removal efficiency loss over time.

Table 7. Kinetic parameters for the Korsmeyer-Peppas model that best fit the experimental data describing the loss of removal efficiency (%) over 200 minutes of work of the three columns reported in Figure 6.			
Column	n_{KP}	K_{KP} [a]	R%$_{200\,EXP}$
1	1.1568	3220	9.1
2	1.1508	2908	7.8
3	1.1154	3957	9.5

[a] Korsmeyer-Peppas kinetic constants expressing the rate of the removal efficiency loss of the three columns overtime over 200 minutes of work. A higher value of K corresponded to a lower rate of removal efficiency loss over time.

As reported in Table 7, the removal efficiency of all columns after 200 min in contact with MB solutions was similar despite the presence or absence of H_2O_2 and its concentration. A slightly lower efficiency for column 2, and a slightly higher one for column 3, were observed. K_{KP} values in column 3 of Table 7 confirmed the experimental R% values in column 4. Column 2 demonstrated a higher efficiency loss rate than columns 1 and 3, while column 3 demonstrated an overall lower rate of removal efficiency loss than columns 1 and 2. Moreover, the transport coefficient (n_{KP}) was > 1 (absolute value), thus establishing that the MB absorption/desorption process followed a Super Case II non-diffusional mechanism. In our case, it can be assumed that the progressive loss of removal efficiency of B400 in columns previously treated with H_2O_2 to quench PFRs, could be due to a progressive release of the MB initially absorbed (first fraction). In this regard, since the n_{KP} value was > 1 for all columns, a Super Case II non-diffusional mechanism can be thought for the desorption of MB entrapped in B400. Super Case II mechanism is an extreme form of release occurring via a solvent crazing process and polymer relaxation rather than simple diffusion.

2.3.3. Monitoring the Presence of PFRs in Bamboo-Based Biochar

EPR monitored the PFRs in the biochar for up to 20 months after exposing it to atmospheric oxygen (during experimental procedures) for 4 months. The concentration of radicals in B400 powder decreased by about 84%, from 1.93×10^{19} to 3.3×10^{18} spins/g, indicating an evident decrease in the performance of the radical degradation of MB in the presence of H_2O_2 (Figure 7).

In Figure 8, it is possible to observe that columns 1–3 have a degradation percentage that remained high even after 5 reuse cycles. On the contrary, columns 4–6, filled with oxygen-exposed BC, demonstrated a significant decrease in the biomass degradation capacity. This phenomenon was caused by the significant decrease in PFRs over time, mainly due to exposure to air and oxygen,[11] as confirmed by the EPR analyses (Figure 7). The reduction of PFRs concentration led to a decrease in the R% of about 60% after 5 cycles, thus confirming that a radical mechanism remarkably supported MB removal by fresh BC via PFRs-mediated ROS production.

To better understand the incidence of an adsorption mechanism in the removal action of B400 and neglect a radical degradation process, an experiment was performed using the aged biochar and an MB solution containing *tert*-butanol as a scavenger of the residual hydroxyl radicals. Results are shown in Figure 9 and compared with those previously obtained with fresh B400.

The results in Figure 9 show a difference in the removal efficiency between columns filled with unexposed B400, those filled with aged B400, and column 7, in which MB solution was prepared with TBA as a scavenger agent. By the third cycle, the difference between columns 1–3 and 7 was around 70%, thus further confirming the previous assumptions.
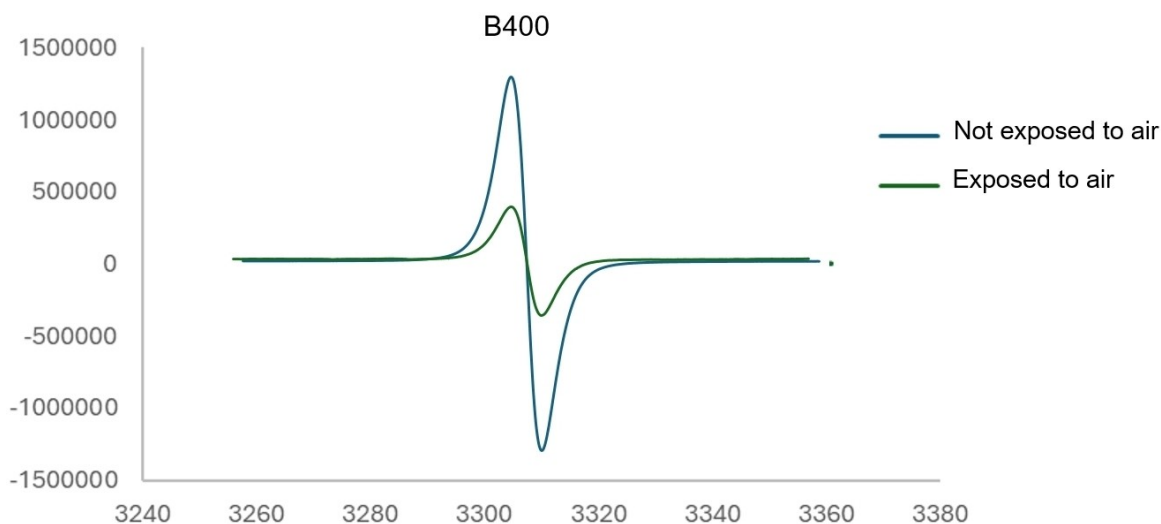
ChemCatChem

Research Article
doi.org/10.1002/cctc.202401042

Chemistry
Europe
European Chemical
Societies Publishing

Figure 7. Comparison of the EPR spectra of B400 stored for 16 months without air exposition and after atmospheric oxygen exposition (4 months).
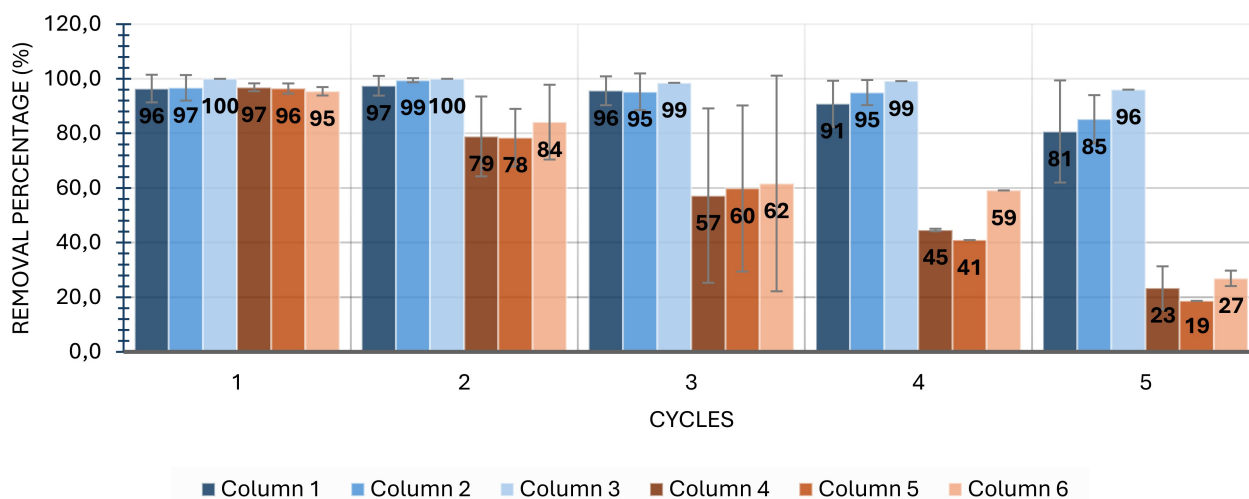

Figure 8. Comparison of MB removal percentage using not exposed to air biochar (columns 1–3), with that using aged biochar (columns 4–6) exposed to oxygen during previous investigations.
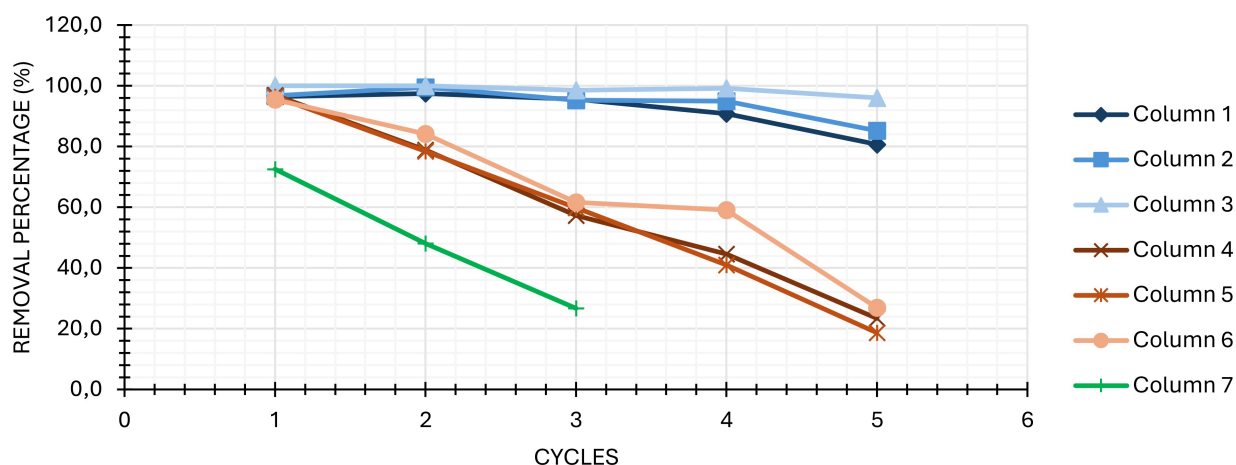

Figure 9. Comparison between the MB removal percentage of those not exposed to air B400 (columns 1–3) and those exposed to air B400 (columns 4–6). In the experiment performed using column 7, TBA as a scavenger agent was used to dilute the MB stock solution.

ChemCatChem

Research Article
doi.org/10.1002/cctc.202401042

Chemistry Europe
European Chemical
Societies Publishing

Although the PFRs-catalysed oxidative process was demonstrated, we also recognise the critical role of the absorption phenomena in the degradation of MB by B400. ROSs, particularly the hydroxyl radical ($^{\bullet}$OH), are unstable compounds with a half-life of nanoseconds. Therefore, to efficiently remove MB owing to a PFRs-catalysed oxidative degradation by ROS, the organic compound's physical absorption on B400 is necessary for allowing the intimate contact of the organic compound with ROS generated by PFRs before their decay. In this way, the generation of the radical species occurs close to the carbon surface where MB is absorbed, and they are ready to act before the quenching. The oxidative phenomena free the BC surface by MB, which can absorb other molecules of not degraded MB in a circular tandem action.

2.3.3.1. Kinetic Study

Data shown in Figure 9 were kinetically studied to confirm the above-reported assertions. According to R^2 values reported in Table S4, while the MB removal data by the first free columns filled with fresh B400 were best modelled by PSO kinetics, which imply chemical reactions including radical processes, those of the columns containing the aged biochar and column 7 well fit the zero order and Higuchi kinetic models at best, but also Hixson Crowell kinetics (Table S3 and Figure S15–S17), which imply physic diffusional mechanisms and B400 surface alteration over time.[65] These results confirmed that not air-exposed fresh BC removed MB mainly by radical degradative oxidation via PFRs-mediated electron transfer to oxygen and H_2O_2 and ROS formation. On the contrary, aged BC in columns 4, 5 and 6, having a low concentration of PFRs due to air exposure, removed MB mainly based on its absorption capacity, which led to an early saturation and a remarkable loss in removal efficiency. Notably, the MB removal by column 7 in the presence of the scavenger, where a radical degradative mechanism was impossible, best fit the Higuchi diffusional model to the highest extent. Kinetic parameters were computed according to the kinetic equations in Table 3 and the equations (blue series) in Figure S115 for columns 1–3, brown and light brown equations in Figure S16 for columns 4 and 5, as well as the pink and green equations in Figure S17 for columns 6 and 7. The results were included in Table 8 together with the experimental R% values at a maximum time of 600 minutes

(R% 600 EXP), which, in the case of columns 1–3, were compared with those provided by the PSO model (R% $_{600\ PSO}$).

As observable in Table 8 and Figure S18, R% values computed by PSO model perfectly agreed with the experimental ones determined after 600 minutes of MB solution treatment. This finding further validated the suitability of PSO model, implying electron transfer reactions, to describe the MB removal process catalysed by PFR in fresh B400. Higher K values corresponded to lower rates of removal efficiency loss over time. As expected, among the columns filled with not exposed B400, column 3 removal efficiency decreased slower than that of columns 1 and 2, while among the columns filled with exposed B400, following the zero-order kinetics, column 1 removal efficiency decreased faster than that of column 2.

3. Conclusions

In this study, we have prepared and characterised bamboo-derived biochar by pyrolytic treatment of bamboo biomass at 400 °C (B400) and demonstrated the rich presence of carbon-centred persistent free radicals (PFRs) stable for 16 months when protected by atmospheric oxygens. Then, we have shown the physical absorption and synergistic PFRs-catalysed oxidative degradation capacity of B400 in removing MB from aqueous solutions. To this end, unlike the most published paper reporting batch tests with homogenous and tedious discontinuous methods, we set up a not commonly reported fix-bed column system filled with B400 to remove MB in a continuous flow. Kinetical studies have been applied to demonstrate the coexistence of adsorption onto BC carbon surface and PFRs-mediated radical electron transfer to atmospheric O_2 and H_2O_2, leading to ROS formation of $^{\bullet}$OH, as tandem mechanisms governing the MB degradative removal from water. The EPR monitoring analysis demonstrated the decrease of radicals' concentration as a direct consequence of the minor efficiency removal of organic dye. A sustainable and low-cost bamboo-based biochar production without any physical and chemical treatment, which could be detrimental to the environment due to the associated chemical waste residuals, has been disclosed with a potential scaling-up production for industrial application. Pilot- or large-scale experiments will be considered by numbering up the fix-bed flow system with real waters or wastewater where the medium's complexity could affect adsorption and advanced oxidative process (AOP). Future work will be dedicated to drug degradation in water, where the catalytic action of BBC-related PFRs should promote ROS-mediated radical and non-radical oxidative reactions leading to the inactivation of complex organic molecules possibly dangerous to the environment.

Supplementary Information Summary

The Electronic Supplementary Information (ESI) includes the data supporting this article. The following data: Raman spectra, elemental analysis, and kinetic studies

Table 8. Kinetic parameters of zero order, PSO and Higuchi models.

Column	K_0	R% $_{600\ EXP}$	R% $_{600\ PSO}$	K_{PSO}	K_H
1	N.A.	81	79	0.0018	N.A.
2	N.A.	85	84	0.0023	N.A.
3	N.A.	96	96	0.0070	N.A.
4	0.9061	23	N.A.	N.A.	5.395
5	0.9651	19	N.A.	N.A.	5.6648
6	N.A.	27	N.A.	N.A.	4.7208
7	1.1458	27	N.A.	N.A.	5.6995

ChemCatChem

Research Article
doi.org/10.1002/cctc.202401042

Chemistry
Europe
European Chemical
Societies Publishing

Author Contributions

Funding

Acknowledgements

Conflict of Interests

The authors declare no conflicts of interest.

Data Availability Statement

The data that support the findings of this study are openly available in Bamboo Biochar-PFR at https://doi.org/[Bamboo Biochar-PFR], reference number 2024.

[1] W. J. Liu, H. Jiang, H. Q. Yu, *Chem. Rev.* **2015**, *115*, 12251–12285.
[2] S. Yu, L. Wang, Q. Li, Y. Zhang, H. Zhou, *Mater. Today Sustain.* **2022**, *19*, 100209.
[3] X. Xiao, B. Chen, Z. Chen, L. Zhu, J. L. Schnoor, *Environ. Sci. Technol.* **2018**, *52*, 5027–5047.
[4] K. Luo, Y. Pang, D. Wang, X. Li, L. Wang, M. Lei, Q. Huang, Q. Yang, *J. Environ. Sci.* **2021**, *108*, 201–216.
[5] M. F. Gasim, Z.-Y. Choong, P.-L. Koo, S.-C. Low, M.-H. Abdurahman, Y.-C. Ho, M. Mohamad, I. W. K. Suryawan, J.-W. Lim, W.-D. Oh, *Catalysts* **2022**, *12*, 210.
[6] Z. Z. Bao, C. Shi, W. Tu, L. Li, Q. Li, *Environ. Pollut.* **2022**, *313*, 120184.
[7] Z. Liu, Z. Xu, L. Xu, F. Buyong, T. C. Chay, Z. Li, Y. Cai, B. Hu, Y. Zhu, X. Wang, *Carbon Res.* **2022**, *1*, 8.
[8] T. G. Ambaye, M. Vaccari, E. D. van Hullebusch, A. Amrane, S. Rtimi, *Int. J. Environ. Sci. Technol.* **2021**, *18*, 3273–3294.
[9] Z. Wang, D. Shen, C. Wu, S. Gu, *Green Chem.* **2018**, *20*, 5031–5057.
[10] S. De, A. M. Balu, J. C. Van Der Waal, R. Luque, *ChemCatChem* **2015**, *7*, 1608–1629.
[11] S. Alfei, O. G. Pandoli, *Toxics* **2024**, *12*, 245.
[12] S. Alfei, O. G. Pandoli, *J. Xenobiot.* **2024**, *14*, 416–451.
[13] J. Yang, J. J. Pignatello, B. Pan, B. Xing, *Environ. Sci. Technol.* **2017**, *51*, 8972–8980.
[14] G. Fang, J. Gao, C. Liu, D. D. Dionysiou, Y. Wang, D. Zhou, *Environ. Sci. Technol.* **2014**, *48*, 1902–1910.
[15] J. Yang, B. Pan, H. Li, S. Liao, D. Zhang, M. Wu, B. Xing, *Environ. Sci. Technol.* **2016**, *50*, 694–700.
[16] Z. Kang, X. Jia, Y. Zhang, X. Kang, M. Ge, D. Liu, C. Wang, Z. He, *Sustainability* **2022**, *14*, 10128.
[17] K. Luo, Q. Yang, Y. Pang, D. Wang, X. Li, M. Lei, Q. Huang, *Chem. Eng. J.* **2019**, *374*, 520–530.
[18] B. W. Lv, H. Xu, J. Z. Guo, L. Q. Bai, B. Li, *J. Hazard. Mater.* **2022**, *421*, 126741.
[19] F. Zhou, K. Li, F. Hang, Z. Zhang, P. Chen, L. Wei, C. Xie, *RSC Adv.* **2022**, *12*, 1885–1896.
[20] F. J. Chacón, M. L. Cayuela, A. Roig, M. A. Sánchez-Monedero, *Rev. Environ. Sci. Biotechnol.* **2017**, *16*, 695–715.
[21] A. Prévoteau, F. Ronsse, I. Cid, P. Boeckx, K. Rabaey, *Sci. Rep.* **2016**, *6*, 32870.
[22] L. Klüpfel, M. Keiluweit, M. Kleber, M. Sander, *Environ. Sci. Technol.* **2014**, *48*, 5601–5611.
[23] X. Zhou, Y. Zhu, Q. Niu, G. Zeng, C. Lai, S. Liu, D. Huang, L. Qin, X. Liu, B. Li, et al., *Chem. Eng. J.* **2021**, *416*, 129027.
[24] J. Du, S. Hoon Kim, M. Azher Hassan, S. Irshad, J. Bao, *Environ. Sci. Pollut. Res. Int.* **2020**, *27*, 37286–37312..
[25] H. Jiang, H. Chen, Z. Duan, Z. Huang, K. Wei, *J. Hazard. Mater. Adv.* **2023**, *10*, 100305.
[26] Y. Wang, X. Gu, Y. Huang, Z. Ding, Y. Chen, X. Hu, *RSC Adv.* **2022**, *12*, 19318–19326.
[27] D. Chen, J. Xu, P. Ling, Z. Fang, Q. Ren, K. Xu, L. Jiang, Y. Wang, S. Su, S. Hu, et al., *Fuel* **2024**, *357*, 129910.
[28] W. Tao, P. Zhang, H. Li, Q. Yang, P. Oleszczuk, B. Pan, *Environ. Sci. Technol.* **2022**, *56*, 10638–10645.
[29] D. Huang, H. Luo, C. Zhang, G. Zeng, C. Lai, M. Cheng, R. Wang, R. Deng, W. Xue, X. Gong, et al., *Chem. Eng. J.* **2019**, *361*, 353–363.
[30] Y. Zhang, M. Xu, R. He, J. Zhao, W. Kang, J. Lv, *Chemosphere* **2022**, *294*, 133737.
[31] Z. Wang, X. Lin, K. Yang, D. Lin, *Water Res.* **2024**, *251*, 121174.
[32] Y. Lin, Q. Ge, J. Wan, Y. Wang, C. Zhu, *Sci. Total Environ.* **2024**, *907*, 168101.
[33] R. Zhang, R. Zhang, A. R. Zimmerman, H. Wang, B. Gao, *Environ. Pollut.* **2023**, *327*, 121543.
[34] E. S. Odinga, M. G. Waigi, F. O. Gudda, J. Wang, B. Yang, X. Hu, S. Li, Y. Gao, *Environ. Int.* **2020**, *134*, 105172.
[35] E. P. Vejerano, G. Rao, L. Khachatryan, S. A. Cormier, S. Lomnicki, *Environ. Sci. Technol.* **2018**, *52*, 2468–2481.
[36] F. Guan, J. Wen, J. Liu, Y. Yuan, S. Zhou, *Environ. Sci. Technol. Lett.* **2023**, *10*, 46–51.
[37] Q. Zhang, R. J. Somerville, L. Chen, Y. Yu, Z. Fei, S. Wang, P. J. Dyson, D. Min, *J. Hazard. Mater.* **2023**, *443*, 1302740.
[38] D. Kalderis, A. Seifi, T. Kieu Trang, T. Tsubota, I. Anastopoulos, I. Manariotis, I. Pashalidis, A. Khataee, *Environ. Res.* **2023**, *224*, 115533.
[39] P. Liao, Z. Malik Ismael, W. Zhang, S. Yuan, M. Tong, K. Wang, J. Bao, *Chem. Eng. J.* **2012**, *195–196*, 339–346.
[40] D. S. de Sá, R. de Andrade Bustamante, C. E. Rodrigues Rocha, V. D. da Silva, E. J. da Rocha Rodrigues, C. Djenne Buarque Müller, K. Ghavami, A. Massi, O. Ginoble Pandoli, *ACS Sustain. Chem. Eng.* **2019**, *7*, 3267–3273.
[41] L. O. L. Gontijo, M. N. B. Junior, D. Santos de Sá, S. Letichevsky, M. J. Pedrozo-Peñafiel, R. Q. Aucélio, I. S. Bott, H. Diniz Lopes Alves, B. Fragneaud, I. Oliveira Maciel, et al., *Carbon* **2023**, *213*, 118214.
[42] E. G. Marina Brustolon, *Electron Paramagnetic Resonance* (Eds: M. Brustolon, E. Giamello), Wiley **2009**.
[43] A. J. Fielding, P. Franchi, B. P. Roberts, T. M. Smits, *J. Chem. Soc. Perkin Trans.* **2002**, *2*, 155–163.
[44] W. Gehling, B. Dellinger, *Environ. Sci. Technol.* **2013**, *47*, 8172–8178.
[45] X. Ruan, Y. Sun, W. Du, Y. Tang, Q. Liu, Z. Zhang, W. Doherty, R. L. Frost, G. Qian, D. C. W. Tsang, *Bioresour. Technol.* **2019**, *281*, 457–468.
[46] Y. Xu, G. Lu, G. Su, X. Chen, J. Meng, Q. Li, C. Wang, B. Shi, *J. Hazard Mater.* **2023**, *456*, 131674.
[47] H. Jia, G. Nulaji, H. Gao, F. Wang, Y. Zhu, C. Wang, *Environ. Sci. Technol.* **2016**, *50*, 6310–6319.

[48] S. Tamamura, T. Sato, Y. Ota, N. Tang, K. Hayakawa, *Acta Geol. Sin. English Ed* **2010**, *80*, 185–191.

[49] James Ashenhurst 3 Factors That Stabilize Free Radicals Available online: https://www.masterorganicchemistry.com/2013/08/02/3-factors-that-stabilize-free-radicals/ (accessed on 19 July 2024).

[50] B. Tang, J. Zhao, J.-F. Xu, X. Zhang, *Chem. Sci.* **2020**, *11*, 1192–1204.

[51] H. Jia, S. Zhao, Y. Shi, K. Zhu, P. Gao, L. Zhu, *J. Hazard Mater.* **2019**, *362*, 92–98.

[52] J. Yuan, Y. Wen, D. D. Dionysiou, V. K. Sharma, X. Ma, *Chem. Eng. J.* **2022**, *429*, 132313.

[53] Y. Wang, X. Gu, Y. Huang, Z. Ding, Y. Chen, X. Hu, *RSC Adv.* **2022**, *12*, 19318–19326.

[54] L. O. L. Gontijo, M. N. Barbosa Junior, D. Santos de Sá, S. Letichevsky, M. J. Pedrozo-Peñafiel, R. Q. Aucélio, I. S. Bott, H. Diniz Lopes Alves, B. Fragneaud, I. Oliveira Maciel, et al., *Carbon* **2023**, *213*, 118214.

[55] J. Yang, J. J. Pignatello, B. Pan, B. Xing, *Environ. Sci. Technol.* **2017**, *51*, 8972–8980.

[56] D. S. de Sá, L. E. Vasconcellos, J. R. de Souza, B. A. Marinkovic, T. Del Rosso, D. Fulvio, D. Maza, A. Massi, O. Pandoli, *J. Photochem. Photobiol. A Chem.* **2018**, *364*, 59–75.

[57] D. S. De Sá, B. A. Marinkovic, E. C. Romani, T. Del Rosso, R. O. M. A. de Souza, A. Massi, O. Pandoli, *J. Flow Chem.* **2016**, *6*, 101–109.

[58] C. Mircioiu, V. Voicu, V. Anuta, A. Tudose, C. Celia, D. Paolino, M. Fresta, R. Sandulovici, I. Mircioiu, *Pharmaceutics* **2019**, *11*, 140.

[59] Mathematical Models of Drug Release. In *Strategies to Modify the Drug Release from Pharmaceutical Systems*, Elsevier **2015**; 63–86.

[60] S. Alfei, V. Orlandi, F. Grasso, R. Boggia, G. Zuccari, *Toxics* **2023**, *11*, 312.

[61] S. Alfei, V. Orlandi, F. Grasso, R. Boggia, G. Zuccari, *Toxics* **2023**, *11*, 312.

[62] J. Luo, Y. Gao, T. Song, Y. Chen, *Water Sci. Technol.* **2021**, *83*, 2327–2344.

[63] X. Teng, J. Li, Z. Wang, Z. Wei, C. Chen, K. Du, C. Zhao, G. Yang, Y. Li, *RSC Adv.* **2020**, *10*, 24712–24720.

[64] X. Liu, Z. Chen, S. Lu, X. Shi, F. Qu, D. Cheng, W. Wei, H. K. Shon, B.-J. Ni, *Water Res.* **2024**, *250*, 120999.

[65] L. Pourtalebi Jahromi, M. Ghazali, H. Ashrafi, A. Azadi, *Heliyon* **2020**, *6*, e03451.

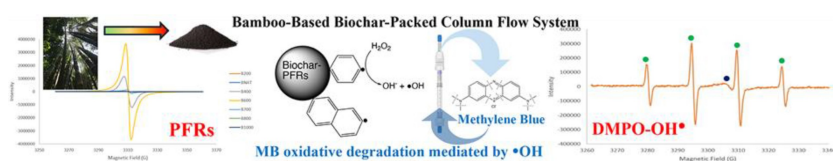[66] I. Y. Wu, S. Bala, N. Škalko-Basnet, M. P. di Cagno, *Eur. J. Pharm. Sci.* **2019**, *138*, 105026.

RESEARCH ARTICLE

Electron paramagnetic resonance (EPR) is used to investigate the stability of Permanent Free Radicals (PFRs) in bamboo biochar generated by pyrolysis of lignocellulose biomass at 400 °C. A bamboo-based biochar-packed flow system is set up for monitoring the oxidative degradation of methylene blue (MB) mediated by the hydroxyl radical (•OH). MB removal profiles are described by a pseudo-second-order kinetic model.

F. Zanardi, F. Romei, M. N. B. Junior, S. Paciornik, P. Franchi, M. Lucarini, A. Turchetti, L. Poletti, S. Alfei*, O. G. Pandoli*

1 – 16

Pivotal Contribute of EPR-Characterized Persistent Free Radicals in the Methylene Blue Removal by a Bamboo-Based Biochar-Packed Column Flow System